Contents lists available at ScienceDirect

Journal of Colloid and Interface Science

journal homepage: http://ees.elsevier.com

Regular Article

Exploring the interplay of mucin with biologically-relevant amorphous magnesium-calcium phosphate nanoparticles

Rita Gelli [a], Francesca Martini [b,d], Marco Geppi [b,d], Silvia Borsacchi [c,d,*], Francesca Ridi [a,*], Piero Baglioni [a]

[a] Department of Chemistry "Ugo Schiff" and CSGI, University of Florence, via della Lastruccia 3, 50019 Sesto Fiorentino, Florence, Italy
[b] Department of Chemistry and Industrial Chemistry, University of Pisa, via G. Moruzzi 13, Pisa 56124, Italy
[c] Institute for the Chemistry of OrganoMetallic Compounds, Italian National Council for Research, CNR-ICCOM Pisa, via G. Moruzzi 1, Pisa 56124, Italy
[d] Center for Instrument Sharing of the University of Pisa (CISUP), Lungarno Pacinotti 43/44, 56126 Pisa, Italy

ARTICLE INFO

Article history:
Received 10 July 2020
Received in revised form 1 February 2021
Accepted 11 March 2021
Available online xxx

Keywords
Amorphous magnesium-calcium phosphate
Nanoparticles
Mucin
Glycoproteins
Gut
Interaction
MAS NMR
Time domain NMR
Spin-spin relaxation

ABSTRACT

Hypothesis: It has been recently shown that, in our organism, the secretions of Ca^{2+}, Mg^{2+} and phosphate ions lead to the precipitation of amorphous magnesium-calcium phosphate nanoparticles.(AMCPs) in the small intestine, where the glycoprotein mucin is one of the most abundant proteins, being the main component of the mucus hydrogel layer covering gut epithelium. Since AMCPs precipitate *in vivo* in a mucin-rich environment, we aim at studying the effect of this glycoprotein on the formation and features of endogenous-like AMCPs.
Experiments: AMCPs were synthesized from aqueous solution in the presence of different concentrations of mucin, and the obtained particles were characterized in terms of crystallinity, composition and morphology. Solid State NMR investigation was also performed in order to assess the interplay between mucin and AMCPs at a sub-nanometric level.
Finding: Results show that AMCPs form in the presence of mucin and the glycoprotein is efficiently incorporated in the amorphous particles. NMR indicates the existence of interactions between AMCPs and mucin, revealing how AMCPs in mucin-hybrid nanoparticles affect the features of both proteic and oligosaccharidic portions of the glycoprotein. Considering that the primary function of mucin is the protection of the intestine from pathogens, we speculate that the nature of the interaction between AMCPs and mucin described in the present work might be relevant to the immune system, suggesting a novel type of scenario which could be investigated by combining physico-chemical and biomedical approaches.

1. Introduction

In the human body, the interaction between organic and inorganic components represents a key aspect which guides the correct functioning of our organism. Notable examples include the role of collagen in the formation of hydroxyapatite nanoplatelets in bone [1] and the interaction between enamel's proteins (amelogenin, ameloblastin and enamelin) and carbonated apatite nanorods in teeth [2]. In physiological conditions, the calcification mainly occurs in hard tissues, whereas in soft tissues and biofluids this phenomenon is limited, mainly due to the action of proteins that, interacting with calcium phosphate nanoclusters during the early stages of formation, prevent their precipitation [3]. Examples include acidic phosphoproteins [4,5] such as caseins in milk, Fetuin-A in serum, statherin in saliva and osteopontin in several biofluids [3]. Sometimes pathological situations due to alterations in organic–inorganic interactions occur, for instance the formation of atherosclerotic plaques in arteries, which results from the co-precipitation of soft molecules (cholesterol, cholesterol esters and phospholipids) and phosphate-based crystals [6,7]. Among the different locations in which physiological calcifications form in our body [8,9], a particularly interesting scenario is represented by the precipitation of amorphous magnesium-calcium phosphate nanoparticles (AMCPs) in the ileum, recently reported by Powell et al. [10]. As depicted in Fig. 1a, the secretion of Ca^{2+} and phosphate ions from the distal small intestine into the lumen leads to the precipitation, together with Mg^{2+}, of porous AMCPs that during their formation can trap antigens and

Abbreviations: AMCP, Amorphous Magnesium-Calcium Phosphate; XRD, X-Rays Diffraction; ATR-FTIR, Attenuated Total Reflectance – Fourier Transform Infrared Spectroscopy; TGA, Thermogravimetry; FE-SEM, Field-Emission Scanning Electron Microscopy; EDX, Energy Dispersive X-Rays Spectroscopy; SSNMR, Solid State Nuclear Magnetic Resonance; MAS, Magic Angle Spinning; Ower, Decoupling; FID, Free Induction Decay HPD: High Power Decoupling; FID, FreeInduction Decay.

* Corresponding authors at: Institute for the Chemistry of OrganoMetallic Compounds, Italian National Council for Research, CNR-ICCOM Pisa, via G. Moruzzi 1, Pisa 56124, Italy (S. Borsacchi). Department of Chemistry "Ugo Schiff" and CSGI, University of Florence, via della Lastruccia 3, Sesto Fiorentino, 50019 Florence, Italy (F. Ridi).
E-mail addresses: silvia.borsacchi@pi.iccom.cnr.it (S. Borsacchi); francesca.ridi@unifi.it (F. Ridi)

https://doi.org/10.1016/j.jcis.2021.03.062
0021-9797/

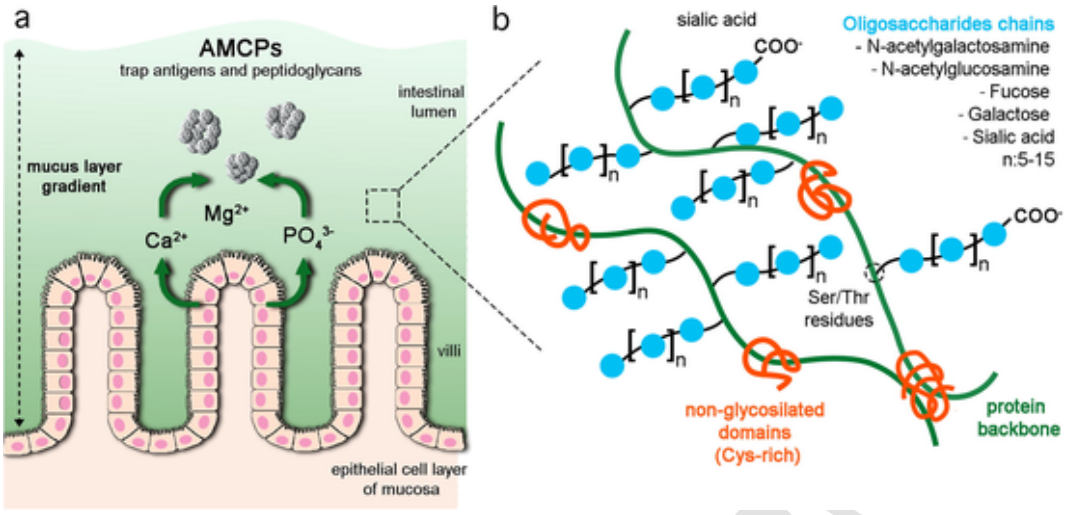

Fig. 1. a) Sketch of AMCP formation pathway in the small intestine, according to the mechanism proposed by Powell et al. [10,11]: the secretions of ions from the distal small intestine into the lumen drive the formation of AMCP nanoparticles. b) Simplified representation of mucin structure (protein components in green and orange, oligosaccharide moieties in blue). (For interpretation of the references to colour in this figure legend, the reader is referred to the web version of this article.)

peptidoglycans, and transport them to the immune cells of the intestinal tissue.

The physiological and pathological implications of this pathway are currently under investigation [12–14], and the features of AMCPs themselves are an interesting topic from a physico-chemical perspective. It was demonstrated that the stability and the features of endogenous-like AMCPs are dependent on the characteristics of the complex fluid in which they form [15,16]. In fact, the intestinal lumen in which AMCPs form is extremely complex and mutable, and many molecules and macromolecules can be encountered during the self-assembly process of these endogenous nanoparticles that can modulate their formation and properties.

One of the most representative components of the intestinal lumen is the mucus hydrogel layer, which forms a diffusion barrier and acts as a protection against the entry in the epithelium of hazardous and infective agents (see Fig. 1a) [17]. The primary structural component of mucus is mucin, a glycoprotein that has a molecular weight of 0.5–20 MDa [18,19]. To date, 21 mucin-type glycoproteins, which collectively belong to the *MUC* gene family, have been identified in the human body, and are divided in two main categories, *i.e.* secreted and cell-bound. Mucins can be found not only in the small intestine but also in the respiratory, reproductive and otolaryngol tracts. All these types of mucins share some common features, and a representative structure is depicted in Fig. 1b. They consist of about 80% by weight of carbohydrates (primarily *N*-acetylgalactosamine, *N*-acetylglucosamine, fucose, galactose, sialic acid and traces of mannose and sulfate), forming oligosaccharide chains of 5–15 monomers attached to the protein core by O-glycosidic bonds to the —OH side groups of serine and threonine [19]. The protein core (20% by weight) consists of two distinct regions: *i)* central glycosylated region rich in serine, threonine and proline (≥60%), and *ii)* non-glycosylated regions rich in cysteine. The formation of S—S disulfide bonds between cysteines leads to a subsequent polymerization of mucin dimers to form multimers. Due to its structure, mucin displays amphiphilic properties in water, as the glycosylated portion is more hydrophilic than the protein core, and it is commonly negatively-charged in physiological conditions [20].

The interest toward mucin properties and applications is rapidly increasing, and the glycoprotein has been used as building block for different types of biomaterials to exploit its barrier properties, hydration and lubrication capabilities, unique chemical diversity and bioactivity [20]. Though the interaction of mucin with different types of nanoparticles has been explored in the literature [21–25], its interplay with calcium phosphate-based nanoparticles was never addressed so far. A few investigations conducted in the nineties report on the effect of mucins from gallbladder on the precipitation of calcium phosphates, which are minor components of gallstones, suggesting mucin affinity for hydroxyapatite [26–30]. A certain affinity of mucin for Mg^{2+} was also reported [31,32]. Taking into account the diffuse distribution of mucin in the intestinal epithelium and lumen, AMCPs will get in contact with such glycoprotein during their formation driven by the endogenous secretions of ions from the distal small intestine into the lumen. With this scenario in mind, the investigation of mucin effect on AMCP formation assumes great relevance and the understanding of their interaction could eventually contribute to unravel the almost unexplored *in vivo* formation mechanism of these particles.

This work reports on synthesized endogenous-like AMCPs in the presence of mucin dispersions (AMCP/mucin). The features of the particles were characterized with a multi-technique approach, including X-rays Diffraction (XRD), Attenuated Total Reflectance–Fourier Transform Infrared Spectroscopy (ATR-FTIR), Thermogravimetry (TGA) and Field-Emission Scanning Electron Microscopy (FE-SEM) coupled with Energy Dispersive X-Rays Spectroscopy (EDX). The interaction between mucin and AMCPs has been characterized in depth carrying out a multinuclear Solid State Nuclear Magnetic Resonance (SSNMR) investigation. NMR has been successfully applied to the deep structural investigation of glycoproteins (including mucin) in solution since the eighties [33–44] but, to the best of our knowledge, NMR studies on solid mucin, and in particular on its interactions with calcium phosphates, have not been reported yet. SSNMR offers the possibility of observing many nuclei and exploiting several nuclear properties sensitive to structure, dynamics and interactions in complex organic, inorganic and organic/inorganic materials [45–50], which appears particularly attractive for trying to understand the complex AMCP/mucin system directly in the solid state. Thus, here we applied a combination of ^{31}P, ^{13}C and ^{1}H high and low-resolution SSNMR techniques to AMCPs, mucin and a representative AMCP/mucin sample. While ^{31}P spectra will allow the characterization of the structural features of AMCPs in the absence or presence of mucin, ^{13}C and ^{1}H experiments will be especially useful for investigating the interactions between mucin and AMCPs.

2. Materials and methods

2.1. Materials

Calcium chloride ($CaCl_2$, ≥93%), magnesium chloride hexahydrate ($MgCl_2{\cdot}6H_2O$, ≥99%), sodium chloride (NaCl, ≥99%) and NaOH pellets were purchased from Sigma-Aldrich (Milan, Italy). Sodium phosphate monobasic ($NaH_2PO_4{\cdot}H_2O$, ≥99%), sodium phosphate dibasic ($Na_2HPO_4{\cdot}12H_2O$, ≥99%) and denatured absolute ethanol were obtained from Carlo Erba Reagents (Milan, Italy). Mucin from porcine stomach, Type II, was also purchased from Sigma-Aldrich. Deionized water was used during all the experiments.

2.2. Synthesis of AMCP in the presence of mucin

AMCPs were prepared by mixing two aqueous solutions at 37 °C, namely 5 mL of solution A ($CaCl_2$ 37.5 mM, $MgCl_2{\cdot}6H_2O$ 25 mM and NaCl 135 mM) and 5 mL of solution B ($NaH_2PO_4{\cdot}H_2O$ 50 mM and $Na_2HPO_4{\cdot}12H_2O$ 150 mM). Mucin was dispersed at 0, 5, 50 and 500 mg in 5 mL of solution A at 37 °C using magnetic stirring, to obtain dispersion at 0, 1, 10 and 100 mg/mL (samples "AMCP", "AMCP_Muc1", "AMCP_Muc10" and "AMCP_Muc100", respectively). Following the dispersion of mucin in solution A, solution B was added, and the pH was adjusted to 7.50 by dropwise addition of NaOH 2 M. The chosen pH value is representative of the ileum's environment [51]. After 15', the reaction medium was centrifuged at 6000 rcf for 3', and the supernatant was discarded. The solid was washed 3 times with denatured ethanol (5 mL of ethanol for the initial 10 mL of reacting solution, with subsequent centrifugation) and dried with N_2 flux and then kept in desiccator using vacuum for 30', to remove ethanol. The obtained samples were stored at −18 °C.

2.3. Characterization methods

2.3.1. X-Rays Diffraction (XRD)

X-rays Diffraction (XRD) patterns were collected with a D8 Advance with DAVINCI design (Bruker, Milan, Italy), using as X-rays source the Cu Kα radiation (wavelength λ = 1.54 Å), at 40 kV and 40 mA. The diffractograms were acquired using a 2θ range of 5°-60°, a step size of 0.03°, and a time/step of 0.3 s. Powder samples were grinded using mortar and pestle and flattened onto a Si zero-background sample holder.

2.3.2. Attenuated Total Reflectance – Fourier Transform Infrared Spectroscopy (ATR-FTIR)

ATR-FTIR spectra were acquired by means of a Nexus Thermo-Nicolet 870 FT-IR spectrophotometer (Madison, WI, USA) equipped with a MCT detector and a Golden Gate. The spectra were collected in the 4000–650 cm^{-1} range, with 128 scans and resolution 2 cm^{-1}.

2.3.3. Thermogravimetry (TGA)

Thermogravimetry measurements were performed using an SDT Q600 from TA Instruments (New Castle, DE, USA). Each sample was placed in an alumina pan and measurements were conducted in N_2 atmosphere (flow rate 100 mL/min) from room temperature to 1000 °C, at 10 °C/min.

2.3.4. Field-Emission Scanning Electron Microscopy (FE-SEM) coupled with Energy Dispersive X-Rays Spectroscopy (EDX)

Field Emission-Scanning Electron Microscopy (FE-SEM) analysis was conducted using a Zeiss ΣIGMA FE-SEM (Carl Zeiss Microscopy GmbH, Jena, Germany). The powders were placed over aluminum stubs by means of conductive tape. The micrographs were acquired with an accelerating voltage of 2 kV, sample-detector distance about 2 mm and using the In-Lens detector. The size distributions were calculated averaging the diameter of 200 particles *per* sample, using the software ImageJ. EDX was carried out using X-act Silicon Drift Detector (Oxford Instruments, England). The accelerating voltage used was 10 kV, while the working distance was about 8 mm. Elemental atomic % ratios are expressed as average ± standard deviation of 5 different sites on each sample.

2.3.5. Solid State Nuclear Magnetic Resonance

Solid State Nuclear Magnetic Resonance (SSNMR) spectra were recorded on a Varian InfinityPlus 400 spectrometer, working at Larmor frequencies of ^1H, ^{13}C and ^{31}P of 400.35, 100.67 and 162.07 MHz, respectively. All the spectra were recorded using a 7.5 mm probehead, under Magic Angle Spinning (MAS) conditions. ^{31}P spectra were recorded with High Power Decoupling from ^1H nuclei (HPD), exploiting Direct Excitation (DE) or Cross-Polarization (CP). ^{31}P DE-MAS spectra were acquired with MAS frequencies of 7 kHz and 6 kHz for samples AMCP and AMCP_Muc10, respectively, and accumulating 1304 transients with a recycle delay of 60 s between two consecutive ones. ^{31}P CP-MAS spectra were recorded with a MAS frequency of 6 kHz, a contact time of 1 ms and accumulating 720 transients with a recycle delay of 3 s. The ^{31}P chemical shift scale was referred to the signal of H_3PO_4 (85%) at 0 ppm. ^{13}C CP-MAS spectra were recorded using a SPINAL-64 [52] pulse sequence for HPD, a MAS frequency of 6 kHz, a linear ramp for the ^{13}C cross-polarization field, a contact time of 2 ms, a recycle delay of 3 s and accumulating 23,000 and 40,000 transients for mucin and AMCP_Muc10, respectively. For mucin a ^{13}C Delayed CP-MAS [53] spectrum was recorded, inserting a delay of 100 μs between the ^1H excitation pulse and the contact pulse, using a MAS frequency of 6 kHz, a contact time of 2 ms, a recycle delay of 3 s and accumulating 80,000 transients. The ^{13}C chemical shift scale was referred to the methyl signal of hexamethylbenzene at 17.35 ppm. ^1H-MAS spectra were recorded at a MAS frequency of 6 kHz, accumulating 40 transients, with a recycle delay of 5 s.

^1H Time Domain SSNMR measurements were performed at a Larmor frequency of 20.8 MHz using a Niumag permanent magnet interfaced with a Stelar PC-NMR console and a 5 mm probe. ^1H Free Induction Decays (FIDs) were recorded on resonance using a solid echo pulse sequence with an echo delay of 14 μs, accumulating 1200 transients for AMCP and AMCP_Muc10, 128 for mucin. The experimental ^1H FID (F(t)) of each sample was directly analyzed by searching the best linear combination of analytical functions (Eq. (1)), chosen among exponential and Gaussian, able to fit it:

$$F(t) = \sum_i w_i f_i(t) \quad (1)$$

Each function f_i represents a motionally distinct fraction of ^1H nuclei, characterized by a spin–spin relaxation time T_{2i} and a weight w_i, corresponding to the percentage of the represented ^1H nuclei. The best linear combination of functions was chosen on the basis of the Occam's Razor principle and of the minimization of the χ^2 of the fitting. T_{2i} and w_i were obtained as fitting parameters [54].

3. Results and discussion

3.1. Characterization of AMCPs prepared in the presence of mucin

The lack of crystallinity of the obtained particles is evidenced by the presence of a broad hump centered at 30° in the XRD pattern, see Fig. 2a, that is diagnostic of amorphous calcium phosphate [55,56]. AMCP_Muc100 also presents a shoulder at lower angles, which is compatible with mucin's pattern that has the highest intensity in this region (see Fig. S1 in the Supplementary Material).

The completely amorphous nature of all samples was confirmed by means of FT-IR spectroscopy (see Fig. 2b). The absorptions, typical of

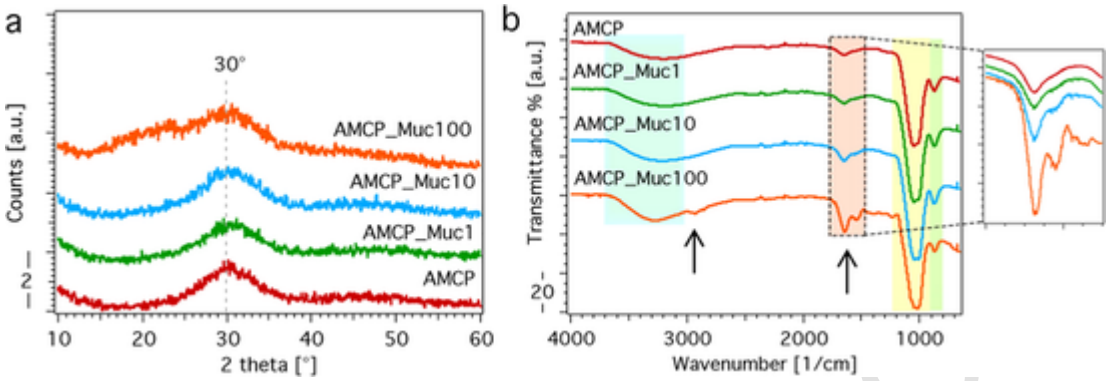

Fig. 2. a) XRD patterns of (from the bottom to the top) AMCP, AMCP_Muc1, AMCP_Muc10 and AMCP_Muc100; b) ATR-FTIR spectra of (from the top to the bottom) AMCP, AMCP_Muc1, AMCP_Muc10 and AMCP_Muc100; the black arrows indicate mucin's signals, whereas the differently-colored regions highlight the main vibrational peaks of AMCP (blue region: O—H stretching, red region: O—H bending, yellow region: P—O stretching, green region: P—O(H) stretching). In the inset: zoom of the region 1300–1900 cm^{-1}. In both graphs, the curves are offset for display purposes. (For interpretation of the references to colour in this figure legend, the reader is referred to the web version of this article.)

phosphate and water vibrations (see Table 1 for the assignments), are quite broad and featureless, consistently with the amorphous nature of the particles [57]. It is worth highlighting that both phosphate and hydrogen-phosphate groups are present in the samples, as shown by the P—O(H) stretching at 1030 and 875 cm^{-1}. This peak, that depends on pH, is not always present in the amorphous calcium phosphate's FT-IR spectra [52,53,54]. In addition to AMCP signals, sample AMCP_Muc100 displays peaks at 2921 cm^{-1}, 2850 cm^{-1}, 1640 cm^{-1} and 1539 cm^{-1}, which reveal the presence of mucin (see Fig. S2) [59]. The analysis of the 1300–1900 cm^{-1} region (Fig. 2b) reveals that also sample AMCP_Muc10 displays mucin's signals, suggesting that a detectable amount of glycoprotein is embedded in both AMCP_Muc10 and AMCP_Muc100.

The amount of mucin present in each sample was determined by means of thermogravimetry. The TGA curves reported in Fig. 3 show, up to 1000 °C, a weight loss of AMCP_Muc1 that is comparable to that of AMCP prepared without mucin (22% for AMCP and 20% for AMCP_Muc1). In contrast, the weight loss of AMCP_Muc10 and AMCP_Muc100 is 30% and 59%, respectively, confirming the presence of the glycoprotein in the samples, likely due to its adsorption on the particles' surface. A TGA analysis of mucin reveals its almost complete degradation upon heating (see Fig. S3, 6% residual weight due to the incomplete pyrolysis in N_2 atmosphere). From these data we can calculate about 11% and 51% of mucin in AMCP_Muc10 and AMCP_Muc100 respectively.

The derivative thermograms, dashed lines in Fig. 3, indicate that the weight loss of AMCP mainly occurs below 100 °C, mainly due to water loss [56,62]. When mucin is also present in the particles, two other peaks in the DTG curves appear (at T = 289 °C and T = 545 °C), which are consistent with the glycoprotein degradation (see Fig. S3).

The morphology of the particles was assessed by FE-SEM, and representative micrographs are shown in Fig. 4. AMCPs are spherical aggregated nanoparticles, whose size is quite heterogeneous (the size distribution curve in the inset in Fig. 4a) with an average diameter of the single objects of 83 ± 24 nm. The presence of mucin in the synthetic medium does not dramatically affect the morphology and the size of the particles. Interestingly, even if some clusters of aggregated mucin are visible in AMCP_Muc100 sample, the surface of some particles appears rough, suggesting that part of mucin coats the surface of AMCPs. In order to inspect if mucin affects the aggregation of the primary particles in solution, the dispersions were analyzed by means of laser granulometry (see Fig. S4): the obtained size distribution curves show that, in all cases, micrometric aggregates are present in solution and their size is not affected by the concentration of the glycoprotein.

In combination with SEM analysis, samples were also analyzed by means of EDX in order to estimate the elemental composition of the particles. The results are reported in Table 2, whereas a representative spectrum can be found in Fig. S5 in the Supplementary Material. Samples prepared with 1 and 10 mg/mL of mucin do not display significant differences from AMCP in all the calculated atomic % ratios (Ca/Mg, Na/Mg, (Ca + Mg)/P and Na/P), except for a slightly higher amount of sodium in AMCP_Muc1. These data were further confirmed by means of Inductively Coupled Plasma Atomic Emission Spectrometry (ICP-OES) measurements coupled with ionic chromatography (data not shown). It is worth noting that if all phosphates were present as PO_4^{3-}, a (Ca + Mg)/P ratio of 1.5 should be obtained. Here, the lower values obtained (close to 1) confirm that some phosphates are present in the particles in hydrogenated form, as already pointed out in FT-IR analysis. We can also hypothesize that some residual phosphate salts from the synthetic medium remained after centrifugation, washing and drying procedure. AMCP_Muc100 shows some differences in composi-

Table 1
FT-IR vibrational peaks of AMCP.

Peak [cm^{-1}]	Assignment	References
875	P—O(H) stretching of protonated phosphates	[60]
1030	P—O stretching	[61]
1653	Water O—H bending	[58]
2700–3700	Water O—H stretching	[58]

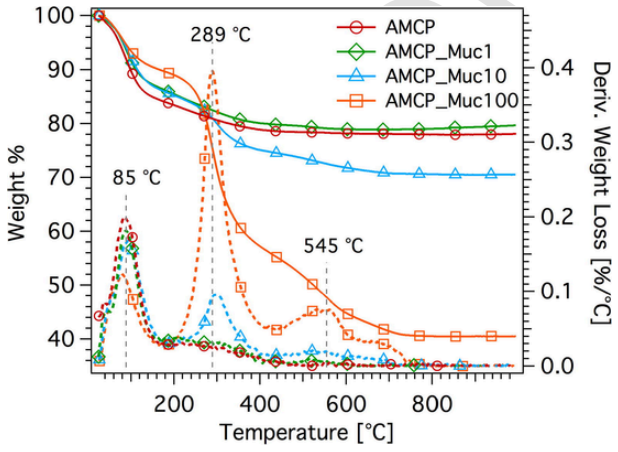

Fig. 3. Thermogravimetry (TGA, solid lines) and derivative thermogravimetric curves (DTG, dashed lines) of AMCP (red, circles), AMCP_Muc1 (diamonds, green), AMCP_Muc10 (triangles, blue) and AMCP_Muc100 (squares, orange). (For interpretation of the references to colour in this figure legend, the reader is referred to the web version of this article.)

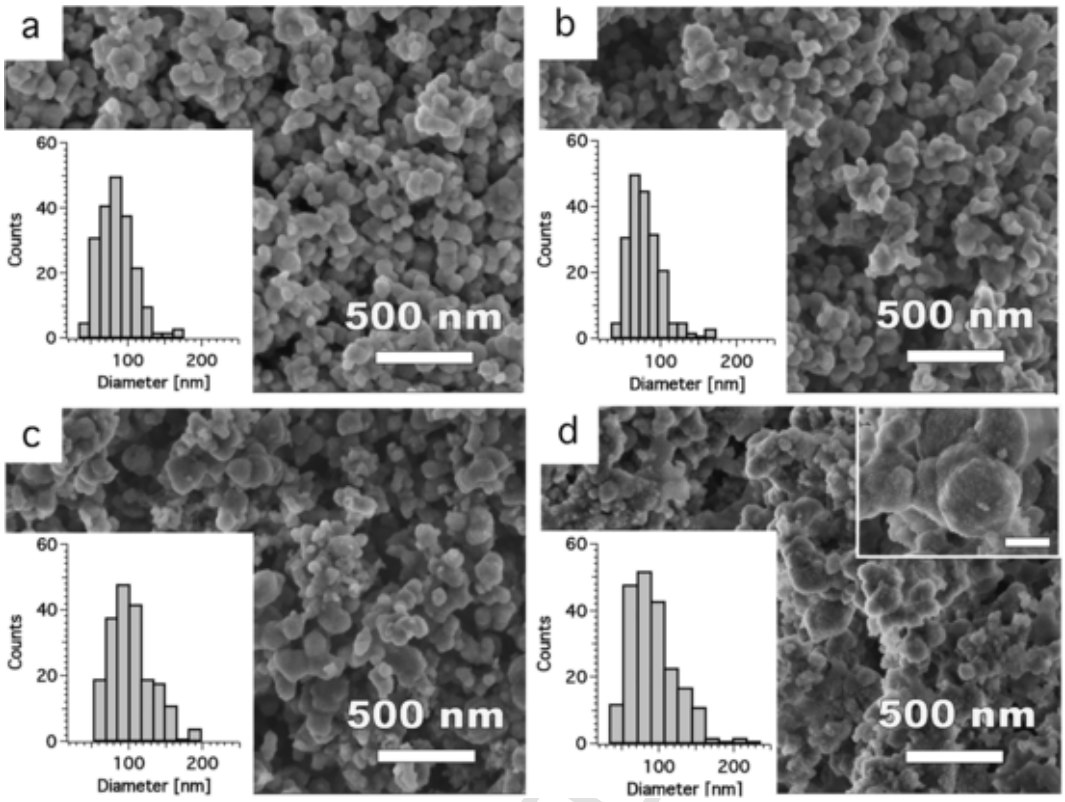

Fig. 4. Representative FE-SEM micrographs of AMCP (a), AMCP_Muc1 (b), AMCP_Muc10 (c), AMCP_Muc_100 (d). In the inset of (d), a detail of the particles is shown (scale bar: 200 nm). In each panel, the size distributions histograms are reported (AMCP: 83 ± 24 nm, AMCP_Muc1: 78 ± 23 nm, AMCP_Muc10: 100 ± 28 nm, AMCP_Muc100: 91 ± 34 nm).

Table 2
Atomic % ratios of the elements composing the samples as obtained by means of EDX.

	Ca/Mg	Na/Mg	(Ca + Mg)/P	Na/P
AMCP	2.35 ± 0.07	1.04 ± 0.07	0.97 ± 0.01	0.30 ± 0.02
AMCP_Muc1	2.4 ± 0.3	1.38 ± 0.03	0.90 ± 0.01	0.36 ± 0.04
AMCP_Muc10	2.42 ± 0.09	1.1 ± 0.3	0.92 ± 0.05	0.30 ± 0.06
AMCP_Muc100	3.9 ± 1.5	1.5 ± 0.2	0.86 ± 0.04	0.3 ± 0.1

tion with respect to the other two samples, likely due to the less effective washing procedure related to the significant amount of protein present in the sample.

Summarizing, AMCPs which mimic the endogenous nanoparticles in terms of composition, morphology, size and crystallinity [10,14] were successfully prepared. The presence of mucin in the synthetic medium in which the particles form does not hamper the formation of endogenous-like particles, and a certain amount is adsorbed on AMCPs' surface or incorporated within the aggregates generated by nanoparticles' agglomeration.

3.2. SSNMR investigation of the interplay between AMCPs and mucin

In order to understand the interplay between AMCPs and mucin, samples AMCP, mucin and AMCP_Muc10 (containing an amount of mucin sufficient to be detectable and sufficiently low not to be in excess) were analyzed by means of a multinuclear SSNMR investigation.

In order to inspect possible structural effects at the sub-nanometric level induced by the presence of mucin on the formation of AMCP, ^{31}P DE-MAS spectra were recorded on AMCP and AMCP_Muc10 (Fig. 5, gray spectra).

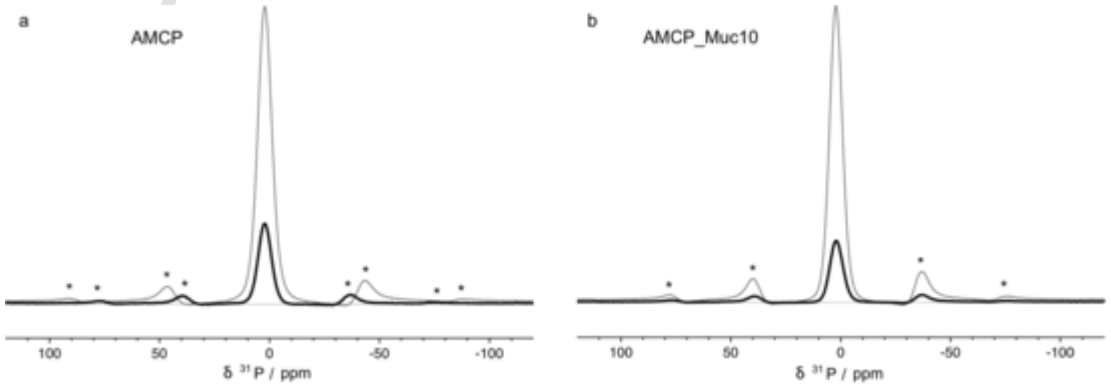

Fig. 5. ^{31}P DE-MAS (gray) and CP-MAS (black) spectra of (a) AMCP (b) AMCP_Muc10. Asterisks indicate spinning sidebands.

The spectra are substantially identical, indicating that the presence of mucin does not markedly affect the formation of AMCPs. In both spectra one isotropic peak is observed, characterized by a chemical shift of 2.1 ppm and a linewidth of about 1200 Hz, and accompanied by a series of spinning sidebands. These features are those already observed for other amorphous calcium phosphates [48,63–68]. The amorphous character is reflected by the distribution of isotropic chemical shifts, resulting in a large linewidth. The only difference that can be found is a slightly smaller linewidth for AMCP_Muc10 (1140 vs 1250 Hz for AMCP), indicating that, in the presence of mucin, AMCP is a little bit more ordered.

The chemical shift at the peak maximum and the presence of spinning sidebands indicate that in both samples PO_4^{3-} groups do not assume, on average, a perfect tetrahedral symmetry and that many of them are partially protonated, in agreement with FT-IR and TGA results.

This is confirmed by ^{31}P CP-MAS spectra (Fig. 5, black spectra), in which ^{31}P signals are built by magnetization transfer from ^{1}H nuclei dipolarly coupled to ^{31}P ones. The signal of AMCP_Muc10 is relatively less intense than that of AMCP (compared with their respective DE-MAS spectra), suggesting that, in the reasonable assumption that ^{31}P relaxation is not modified, when mucin is present phosphate groups have a slightly minor amount of hydrogens strongly dipolarly coupled, *i.e.* covalently bonded hydrogen atoms and/or strongly hydrogen-bonded water.

Direct information on mucin in AMCP_Muc10 has been obtained by exploiting ^{13}C SSNMR.

The ^{13}C CP-MAS spectrum of mucin is shown in Fig. 6. The complexity of the protein makes the spectrum very crowded, preventing a full assignment of the signals, which is however out of the scope of this work. On the other hand, the most important signals can be clearly identified. The oligosaccharide carbons are the main responsible for the signals at 72.0 ppm and 101.4 ppm, and contribute to those at 24, 50, 61 and 173 ppm [34,36,37,69]. All the other signals arise from the protein backbone, mainly constituted by serine, threonine and proline. In agreement with ^{13}C chemical shifts reported in the literature for submaxillary mucins [34,36], peaks at 55 and 59 ppm are ascribable to Cα of serine and proline/threonine, respectively. The signal of proline Cβ appears at 30 ppm, while those of threonine and serine are overlapped to other signals. Cγ of proline and threonine contribute to the broad signal at 24 ppm. Protein carboxylic carbons give rise to the intense signal at 173 ppm. Minor signals can be ascribed to other aminoacids as glycine, oxidized cysteine and arginine (41 ppm), some aromatic aminoacids (130 ppm) and aspartic acid (157 ppm). Moreover, all signals observed and described are also compatible with the presence of other aminoacids that could be present in smaller amounts [34].

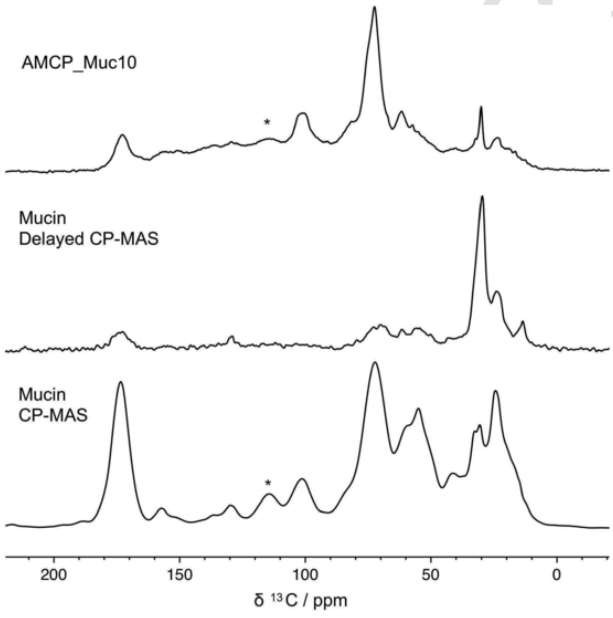

Fig. 6. From bottom to top: ^{13}C CP-MAS and ^{13}C Delayed CP-MAS spectra of mucin, ^{13}C CP-MAS spectrum of AMCP_Muc10. Asterisks indicate spinning sidebands.

The ^{13}C Delayed CP-MAS spectrum, selectively showing signals of carbon nuclei dipolarly coupled to ^{1}H nuclei in mobile environments, shows that both oligosaccharide chains and protein backbone of mucin are very rigid. Indeed, in the selective spectrum most mucin signals are suppressed, with the only exception of peaks at 13, 24 and 30 ppm, ascribable to mobile methyl groups and —CH_2— groups of aminoacid side chains.

When mucin is entrapped in AMCP_Muc10, its ^{13}C CP-MAS spectrum appears different (Fig. 6). In particular, the comparison with the spectrum of mucin highlights on the whole a decrease of the intensity of the signals of the protein backbone, with respect to those of the oligosaccharide chains. This can be ascribed to an increased mobility of the protein backbone, which partially reduces the strength of the ^{1}H–^{13}C dipolar interactions responsible for the creation of the signals in the CP-MAS spectra.

In order to better investigate the dynamics of mucin in AMCP_Muc10, ^{1}H FIDs of mucin, AMCP and AMCP_Muc10 were recorded on resonance and analyzed for determining the ^{1}H spin–spin relaxation times T_2′s, which in solid samples are usually very short (of the order of 10–100 μs) and, out of the so called "rigid lattice regime", monotonically increase with increasing mobility [69,70]. The numerical results of FID analyses are reported in Table 3, while in Fig. 7 it is reported

Table 3
Results of the ^{1}H FID analysis on mucin, AMCP and AMCP_Muc10, expressed as ^{1}H relaxation times T_{2i} and corresponding ^{1}H percentage population (w_i). For AMCP_Muc10 the "theoretical" values ("theor"), estimated as explained in the text, are also reported. Uncertainties on the experimental values are about ± 1%.

	T_{2a} (μs)	w_a (%)	T_{2b} (μs)	w_b (%)	T_{2c} (μs)	w_c (%)
Mucin	15.3	79	83.3	18	937.0	3
AMCP	13.8	64	94.5	36		
AMCP_Muc10	15.0	66	107.0	34		
AMCP_Muc10 "theor"	14.7	73	87.6	25	937.0	2

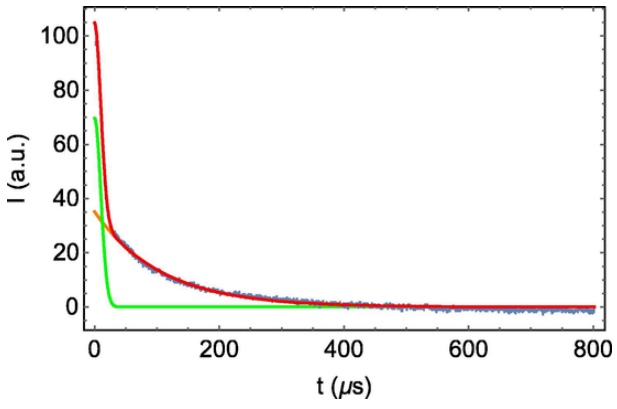

Fig. 7. ^{1}H FID analysis of AMCP_Muc10. The different curves are: experimental (grey) and fitted (red) FID. The fitted FID results from a linear combination of a Gaussian (green) and an exponential (orange) function, representing ^{1}H nuclei with T_{2a} = 15 μs and T_{2b} = 107 μs, respectively (see Table 3). (For interpretation of the references to colour in this figure legend, the reader is referred to the web version of this article.)

as an example the plot of the ^{1}H FID analysis of AMCP_Muc 10 (details of the FID analysis procedure are reported in Section 2.3.5).

The rigidity of mucin, already highlighted by its ^{13}C CP-MAS spectrum, is confirmed: most (80%) of its ^{1}H nuclei have a very short T_2 (15 μs), while the remaining 20% are present in environments with intermediate (T_2 = 83 μs) or high mobility (T_2 = 937 μs) and can be ascribed to methyl and side —CH_2— groups, in agreement with the ^{13}C Delayed CP-MAS spectrum. ^{1}H nuclei of AMCP, which belong to water and P-OH groups, are distributed between a very rigid fraction (T_2 = 14 μs) and a more mobile one (T_2 = 94 μs). Also, AMPC_Muc10 presents two fractions of ^{1}H nuclei in motionally different environments: a prevailing one, very rigid, and a minor one, more mobile. In order to interpret the experimental results of AMCP_Muc10 it is useful to make a comparison with the "theoretical" expected results, calculated in the hypothesis that neither mucin nor AMCP modify their dynamics with respect to the pristine samples. Based on the estimated mucin content of 11 wt% and considering approximate "molecular formulas" for AMCP ($Ca_{2.4}MgNaH_{2.4}(PO_4)_{3.4}{\cdot}5H_2O$, estimated on the basis of EDX and TGA results) and mucin (obtained taking a representative saccharide and aminoacid in a 80:20 wt ratio), "theoretical" T_2 values and weights for AMCP_Muc10 have been estimated and are reported in Table 3. The comparison with the experimental results clearly shows that in passing from pristine mucin and AMCP to AMCP_Muc10, the intermediate T_2 increases and about 7% of ^{1}H nuclei pass from the rigid to the intermediate fraction, which also incorporates the minor amount of very mobile protons. Considering the ^{13}C SSNMR results it is reasonable to assign this 7% of mobilized protons to the mucin protein backbone. Interestingly, according to the composition estimates above mentioned, the hydrogen atoms of the protein backbone would be about 10% of the total hydrogen content of AMCP_Muc10.

A further confirmation of protein mobilization in AMCP_Muc10 arises from ^{1}H-MAS spectra (Fig. 8).

All spectra show a broad intense non-resolved part arising from the strongly dipolar coupled ^{1}H nuclei (roughly corresponding to those with short T_2) and some resolved signals, ascribable to more mobile hydrogens, which are discussed in the following (Fig. 8, right). The spectrum of mucin is dominated by an intense signal at about 1 ppm, ascribable to mobile CH_3 and CH_2 groups in side chains, in agreement with the ^{13}C Delayed CP-MAS spectrum. The spectrum of AMCP shows a broad peak centered at about 5.5 ppm, ascribable to hydrogen-bonded water, while the broad shoulder centered at about 11 ppm arises from P-OH groups [63–65,68] and the two narrow signals at 1 and 3.5 ppm are due to ethanol traces. The spectrum of AMCP_Muc10 resembles that of AMCP, but interestingly in the resolved part of the spectrum a signal at about 4.5 ppm appears, which can be ascribed to protein Hα, hardly visible in the spectrum of mucin due to their rigidity (the assignment to additional bound water, often appearing at this chemical shift, can be ruled out based on TGA results). Even if the evaluation of signal areas cannot be rigorously performed due to the scarce spectral resolution, from a tentative analysis the area of this new peak is about 5% of the whole spectral area, further confirming the hypothesized mobilization of most of the protein backbone in AMCP_Muc10.

The ensemble of ^{13}C and ^{1}H SSNMR results, even if indirectly, point to the establishment of mucin-AMCP interactions, which imply a substantial rigidity of the oligosaccharidic chains, while leaving a major mobility to the protein backbone. This is reasonable considering that the hydrophilic glycans would easily involve their OH groups in hydrogen-bonds with water molecules embedded in the inorganic particles and also with phosphate ions, which, actually, based on ^{31}P SSNMR results, seem less important. Moreover, electrostatic interactions between inorganic cations and negatively charged side groups of glycans (sialic acids) and aminoacids (glutamic and aspartic acids) can give an additional contribution (notably the signal at 30 ppm in the ^{13}C CP-MAS spectrum of AMCP_Muc10, showing a somehow peculiar intensity, could account for Cβ and Cγ of Glu and Asp, which could stiffen due to the interaction with AMCP).

4. Conclusions

The endogenous formation of AMCPs in human's small intestine offers a fascinating scenario with many physico-chemical interesting outcomes [10]. This work is, to the best of our knowledge, the first report about the effect of the glycoprotein mucin, which is the major component of the intestinal mucus, on the features of endogenous-like AMCPs. The analysis was carried out at different structural levels, in the attempt of understanding a possible specific interplay between the inorganic (AMCP) and organic (mucin) components. We succeeded in synthesizing AMCPs with features compatible with the endogenous ones [14], both in the absence and in the presence of different mucin concentrations. Results show that the presence of the glycoprotein in the synthetic medium does not hamper the formation of amorphous particles, nor it affects their morphology at the nano-micro scale. Nevertheless, a significant amount of mucin is present in AMCP_Mucin samples,

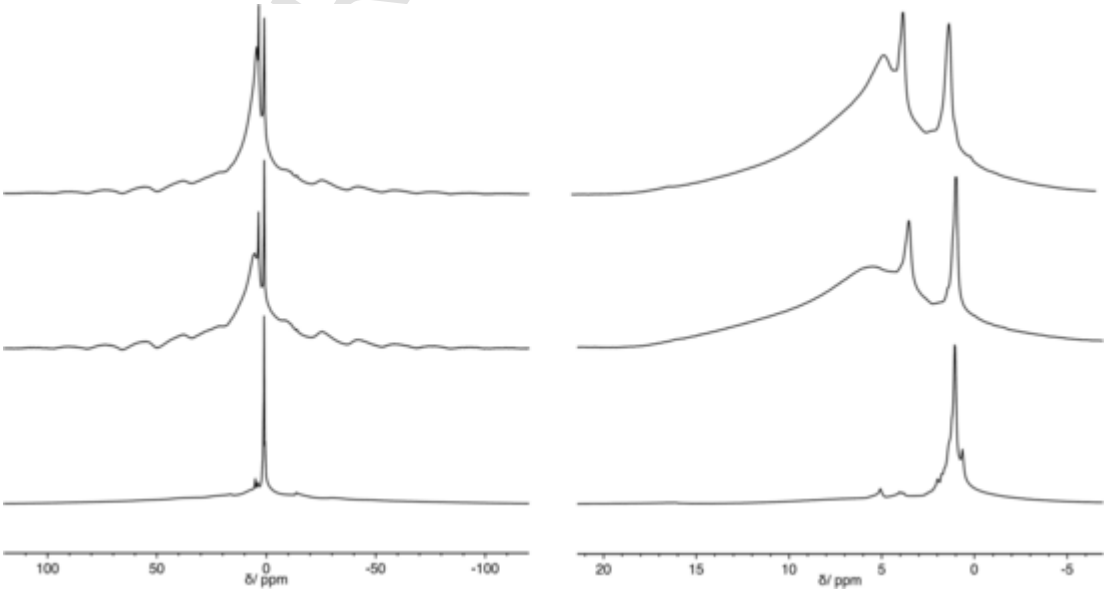

Fig. 8. ^{1}H-MAS spectra (a) full and (b) expanded in the −7 ÷ 21 ppm region of, from bottom to top: mucin, AMCP, AMCP_Muc10.

suggesting an adsorption on particles' surface or an incorporation in the aggregates generated by the nanoparticles. The lack of influence of mucin on the sub-nanometric structure of AMCP primary units was further confirmed by a ^{31}P SSNMR analysis. The combination of ^{13}C and ^{1}H SSNMR experiments, on the other hand, suggests the presence of mucin-AMCP interactions, which imply a substantial rigidity of the oligosaccharidic chains, while leaving a major mobility to the protein backbone. This scenario is compatible with the interaction of AMCPs with the oligosaccharide portion of the glycoprotein, where hydrogen bonding and electrostatic interactions may play a crucial role, likely with the additional contribution of negatively charged side groups of aminoacids.

The results presented in this work show that an interplay between mucin and AMCPs exists at the structural level; besides the relevance in the understanding of the interactions occurring in these biologically-relevant hybrid structures, the obtained results suggest that AMCPs, while forming *in vivo*, might interact with mucin, which is well-distributed in the environment in which the particles self-assemble. Both AMCPs and mucin play a role at the immune system level: the amorphous particles are involved in tolerogenic mechanisms [10], whereas the primary function of mucus layer is the protection of the intestine from pathogens and from our own intestinal microbiota as well (the interplay of mucins with gut microbiota is a topic which has recently gained the attention of the scientific community [71–73]). Interestingly, it was recently hypothesized that mucins might also be involved in tolerogenic mechanisms, this aspect requiring further investigations [17]. In light of these considerations, we can speculate that the nature of the interaction between AMCPs and mucin described in the present work might have a role in shaping their function towards the immune system, suggesting a novel type of scenario which could be investigated by combining physico-chemical and biomedical approaches.

CRediT authorship contribution statement

Rita Gelli: Conceptualization, Investigation, Writing - original draft, Writing - review & editing, Visualization. **Francesca Martini:** Investigation, Writing - review & editing. **Marco Geppi:** Investigation, Writing - review & editing. **Silvia Borsacchi:** Investigation, Writing - original draft, Writing - review & editing. **Francesca Ridi:** Conceptualization, Investigation, Resources, Writing - review & editing. **Piero Baglioni:** Resources, Writing - review & editing, Funding acquisition.

Declaration of Competing Interest

The authors declare that they have no known competing financial interests or personal relationships that could have appeared to influence the work reported in this paper.

Acknowledgements

Fondazione CR Firenze (project 2017.0720), CSGI consortium and MIUR-Italy ("Progetto Dipartimenti di Eccellenza 2018-2022" allocated to Department of Chemistry "Ugo Schiff") are acknowledged for financial support.

Appendix A. Supplementary material

Supplementary data to this article can be found online at https://doi.org/10.1016/j.jcis.2021.03.062.

References

[1] F. Ridi, I. Meazzini, B. Castroflorio, M. Bonini, D. Berti, P. Baglioni, Functional calcium phosphate composites in nanomedicine, Adv. Colloid Interface Sci. 244 (2017) 281–295, doi:10.1016/j.cis.2016.03.006.

[2] J.P. Simmer, P. Papagerakis, C.E. Smith, D.C. Fisher, A.N. Rountrey, L. Zheng, J.-C.-C. Hu, Regulation of dental enamel shape and hardness, J. Dent. Res. 89 (2010) 1024–1038, doi:10.1177/0022034510375829.

[3] S. Lenton, Q. Wang, T. Nylander, S. Teixeira, C. Holt, Structural biology of calcium phosphate nanoclusters sequestered by phosphoproteins, Crystals. 10 (2020) 755, doi:10.3390/cryst10090755.

[4] A. George, A. Veis, Phosphorylated proteins and control over apatite nucleation, crystal growth, and inhibition, Chem. Rev. 108 (2008) 4670–4693, doi:10.1021/cr0782729.

[5] K. Alvares, The role of acidic phosphoproteins in biomineralization, Connect. Tissue Res. 55 (2014) 34–40, doi:10.3109/03008207.2013.867336.

[6] L.N. Poloni, M.D. Ward, The materials science of pathological crystals, Chem. Mater. 26 (2014) 477–495, doi:10.1021/cm402552v.

[7] S.V. Dorozhkin, M. Epple, Biological and medical significance of calcium phosphates, Angew. Chem. Int. Ed. 41 (2002) 3130–3146, doi:10.1002/1521-3773(20020902)41:17<3130::AID-ANIE3130>3.0.CO;2-1.

[8] E. Königsberger, L. Königsberger, (Eds.), Biomineralization: Medical Aspects of Solubility, J. Wiley, Chichester, England ; Hoboken, NJ, 2006.

[9] R. Gelli, F. Ridi, P. Baglioni, The importance of being amorphous: calcium and magnesium phosphates in the human body, Adv. Colloid Interface Sci. 269 (2019) 219–235, doi:10.1016/j.cis.2019.04.011.

[10] J.J. Powell, E. Thomas-McKay, V. Thoree, J. Robertson, R.E. Hewitt, J.N. Skepper, A. Brown, J.C. Hernandez-Garrido, P.A. Midgley, I. Gomez-Morilla, G.W. Grime, K.J. Kirkby, N.A. Mabbott, D.S. Donaldson, I.R. Williams, D. Rios, S.E. Girardin, C.T. Haas, S.F.A. Bruggraber, J.D. Laman, Y. Tanriver, G. Lombardi, R. Lechler, R.P.H. Thompson, L.C. Pele, An endogenous nanomineral chaperones luminal antigen and peptidoglycan to intestinal immune cells, Nat. Nanotechnol. 10 (2015) 361–369, doi:10.1038/nnano.2015.19.

[11] J.D. Söderholm, Gut immunology: Nanoparticles ferry gut antigens, Nat. Nanotechnol. 10 (2015) 298–299, doi:10.1038/nnano.2015.58.

[12] J. Robertson, C.T. Haas, L.C. Pele, T.P. Monie, C. Charalambos, M. Parkes, R.E. Hewitt, J.J. Powell, Intestinal APCs of the endogenous nanomineral pathway fail to express PD-L1 in Crohn's disease, Sci. Rep. 6 (2016), doi:10.1038/srep26747.

[13] R.E. Hewitt, J. Robertson, C.T. Haas, L.C. Pele, J.J. Powell, Reduction of T-helper cell responses to recall antigen mediated by codelivery with peptidoglycan via the intestinal nanomineral-antigen pathway, Front. Immunol. 8 (2017), doi:10.3389/fimmu.2017.00284.

[14] L.C. Pele, C.T. Haas, R.E. Hewitt, J. Robertson, J. Skepper, A. Brown, J.C. Hernandez-Garrido, P.A. Midgley, N. Faria, H. Chappell, J.J. Powell, Synthetic mimetics of the endogenous gastrointestinal nanomineral: Silent constructs that trap macromolecules for intracellular delivery, Nanomedicine Nanotechnol. Biol. Med. 13 (2017) 619–630, doi:10.1016/j.nano.2016.07.008.

[15] R. Gelli, M. Scudero, L. Gigli, M. Severi, M. Bonini, F. Ridi, P. Baglioni, Effect of pH and Mg2+ on Amorphous Magnesium-Calcium Phosphate (AMCP) stability, J. Colloid Interface Sci. 531 (2018) 681–692, doi:10.1016/j.jcis.2018.07.102.

[16] R. Gelli, P. Tempesti, F. Ridi, P. Baglioni, Formation and properties of amorphous magnesium-calcium phosphate particles in a simulated intestinal fluid, J. Colloid Interface Sci. 546 (2019) 130–138, doi:10.1016/j.jcis.2019.03.060.

[17] M.E.V. Johansson, G.C. Hansson, Immunological aspects of intestinal mucus and mucins, Nat. Rev. Immunol. 16 (2016) 639–649, doi:10.1038/nri.2016.88.

[18] C.E. Wagner, K.M. Wheeler, K. Ribbeck, Mucins and their role in shaping the functions of mucus barriers, Annu. Rev. Cell Dev. Biol. 34 (2018) 189–215, doi:10.1146/annurev-cellbio-100617-062818.

[19] R. Bansil, B.S. Turner, Mucin structure, aggregation, physiological functions and biomedical applications, Curr. Opin. Colloid Interface Sci. 11 (2006) 164–170, doi:10.1016/j.cocis.2005.11.001.

[20] G. Petrou, T. Crouzier, Mucins as multifunctional building blocks of biomaterials, Biomater. Sci. 6 (2018) 2282–2297, doi:10.1039/C8BM00471D.

[21] N. Hendler, L. Fadeev, E.D. Mentovich, B. Belgorodsky, M. Gozin, S. Richter, Bio-inspired synthesis of chiral silver nanoparticles in mucin glycoprotein—the natural choice, Chem. Commun. 47 (2011) 7419–7421, doi:10.1039/C1CC11228G.

[22] B. Belgorodsky, E. Drug, L. Fadeev, N. Hendler, E. Mentovich, M. Gozin, Mucin complexes of nanomaterials: first biochemical encounter, Small Weinh. Bergstr. Ger. 6 (2010) 262–269, doi:10.1002/smll.200900637.

[23] N. Barbero, M. Coletti, F. Catalano, S. Visentin, Exploring gold nanoparticles interaction with mucins: A spectroscopic-based study, Int. J. Pharm. 535 (2018) 438–443, doi:10.1016/j.ijpharm.2017.11.026.

[24] V.N. Boya, R. Lovett, S. Setua, V. Gandhi, P.K.B. Nagesh, S. Khan, M. Jaggi, M.M. Yallapu, S.C. Chauhan, Probing mucin interaction behavior of magnetic nanoparticles, J. Colloid Interface Sci. 488 (2017) 258–268, doi:10.1016/j.jcis.2016.10.090.

[25] P.C. Griffiths, B. Cattoz, M.S. Ibrahim, J.C. Anuonye, Probing the interaction of nanoparticles with mucin for drug delivery applications using dynamic light scattering, Eur. J. Pharm. Biopharm. 97 (2015) 218–222, doi:10.1016/j.ejpb.2015.05.004.

[26] Antoine E. Khoury, Salomon Michael, Doche Roger, Soboh Fouad, Ackerley Cameron, Jayanthi Rama, Gordon A. McLorie, Marc W. Mittelman, Stone formation after augmentation cystoplasty: the role of intestinal mucus, J. Urol. 158 (1997) 1133–1137, doi:10.1016/S0022-5347(01)64404-5.

[27] N.H. Afdhal, J.D. Ostrow, R. Koehler, N. Niu, A.K. Groen, A. Veis, D.P. Nunes, G.D. Offner, Interaction of bovine gallbladder mucin and calcium-binding protein: Effects on calcium phosphate precipitation, Gastroenterology 109 (1995) 1661–1672, doi:10.1016/0016-5085(95)90656-8.

[28] F. Grases, A. Llobera, Experimental model to study sedimentary kidney stones, Micron. 29 (1998) 105–111, doi:10.1016/S0968-4328(98)00006-7.

[29] S.-M. Qiu, G. Wen, J. Wen, R.D. Soloway, R.S. Crowther, Interaction of human gallbladder mucin with calcium hydroxyapatite: Binding studies and the effect

on hydroxyapatite formation, Hepatology 21 (1995) 1618–1624, doi:10.1002/hep.1840210621.
[30] A.A. van den Berg, J.D. van Buul, G.N.J. Tytgat, A.K. Groen, J.D. Ostrow, Mucins and calcium phosphate precipitates additively stimulate cholesterol crystallization, J. Lipid Res. 39 (1998) 1744–1751.
[31] Y. Shan, Q. Xu, M. Ma, Mg2+ binding affects the structure and activity of ovomucin, Int. J. Biol. Macromol. 70 (2014) 230–235, doi:10.1016/j.ijbiomac.2014.06.056.
[32] Y. Jang, D. Owuor, J.T. Waterman, L. White, B. Collins, J. Sankar, T.W. Gilbert, Y. Yun, Effect of Mucin and Bicarbonate Ion on Corrosion Behavior of AZ31 Magnesium Alloy for Airway Stents, Materials. 7 (2014) 5866–5882, doi:10.3390/ma7085866.
[33] H. Van Halbeek, Structural analysis of the carbohydrate chains of mucin-type glycoproteins by high-resolution 1H-n.m.r. spectroscopy, Biochem. Soc. Trans. 12 (1984) 601–605, doi:10.1042/bst0120601.
[34] T.A. Gerken, D.G. Dearborn, Carbon-13 NMR studies of native and modified ovine submaxillary mucin, Biochemistry 23 (1984) 1485–1497, doi:10.1021/bi00302a023.
[35] T.A. Gerken, The solution structure of mucous glycoproteins: Proton NMR studies of native and modified ovine submaxillary mucin, Arch. Biochem. Biophys. 247 (1986) 239–253, doi:10.1016/0003-9861(86)90581-3.
[36] T.A. Gerken, N. Jentoft, Structure and dynamics of porcine submaxillary mucin as determined by natural abundance carbon-13 NMR spectroscopy, Biochemistry 26 (1987) 4689–4699, doi:10.1021/bi00389a015.
[37] M. Paris, H. Bizot, J. Emery, J.Y. Buzaré, A. Buléon, NMR local range investigations in amorphous starchy substrates I. Structural heterogeneity probed by 13C CP–MAS NMR, Int. J. Biol. Macromol. 29 (2001) 127–136, doi:10.1016/S0141-8130(01)00160-X.
[38] J.D. Fontenot, N. Tjandra, D. Bu, C. Ho, R.C. Montelaro, O.J. Finn, Biophysical characterization of one-, two-, and three-tandem repeats of human mucin (muc-1) protein core, Cancer Res. 53 (1993) 5386–5394.
[39] M.R. Wormald, A.J. Petrescu, Y.-L. Pao, A. Glithero, T. Elliott, R.A. Dwek, Conformational studies of oligosaccharides and glycopeptides: complementarity of NMR, X-ray crystallography, and molecular modelling, Chem. Rev. 102 (2002) 371–386, doi:10.1021/cr990368i.
[40] D.M. Coltart, A.K. Royyuru, L.J. Williams, P.W. Glunz, D. Sames, S.D. Kuduk, J.B. Schwarz, X.-T. Chen, S.J. Danishefsky, D.H. Live, Principles of mucin architecture: structural studies on synthetic glycopeptides bearing clustered mono-, Di-, Tri-, and hexasaccharide glycodomains, J. Am. Chem. Soc. 124 (2002) 9833–9844, doi:10.1021/ja020208f.
[41] C. Robbe, C. Capon, E. Maes, M. Rousset, A. Zweibaum, J.-P. Zanetta, J.-C. Michalski, Evidence of regio-specific glycosylation in human intestinal mucins Presence of an acidic gradient along the intestinal tract, J. Biol. Chem. 278 (2003) 46337–46348, doi:10.1074/jbc.M302529200.
[42] G. Lafitte, O. Söderman, K. Thuresson, J. Davies, PFG-NMR diffusometry: A tool for investigating the structure and dynamics of noncommercial purified pig gastric mucin in a wide range of concentrations, Biopolymers 86 (2007) 165–175, doi:10.1002/bip.20717.
[43] J.J. Barchi, Mucin-type glycopeptide structure in solution: past, present, and future, Biopolymers. 99 (2013) 713–723, doi:10.1002/bip.22313.
[44] F. Marcelo, F. Garcia-Martin, T. Matsushita, J. Sardinha, H. Coelho, A. Oude-Vrielink, C. Koller, S. André, E.J. Cabrita, H.-J. Gabius, S.-I. Nishimura, J. Jiménez-Barbero, F.J. Cañada, Delineating Binding modes of Gal/GalNAc and structural elements of the molecular recognition of tumor-associated mucin glycopeptides by the human macrophage galactose-type lectin, Chem. – Eur. J. 20 (2014) 16147–16155, doi:10.1002/chem.201404566.
[45] M. Geppi, S. Borsacchi, G. Mollica, C.A. Veracini, Applications of solid-state NMR to the study of organic/inorganic multicomponent materials, Appl. Spectrosc. Rev. 44 (2008) 1–89, doi:10.1080/05704920802352564.
[46] E. Cappelletto, S. Borsacchi, M. Geppi, F. Ridi, E. Fratini, P. Baglioni, Comb-shaped polymers as nanostructure modifiers of calcium silicate hydrate: A ^{29} Si solid-state NMR investigation, J. Phys. Chem. C. 117 (2013) 22947–22953, doi:10.1021/jp407740t.
[47] F. Martini, S. Borsacchi, M. Geppi, G. Ruggeri, A. Pucci, Understanding the aggregation of bis(benzoxazolyl)stilbene in PLA/PBS blends: a combined spectrofluorimetric, calorimetric and solid state NMR approach, Polym. Chem. 5 (2013) 828–835, doi:10.1039/C3PY01039B.
[48] M. Tonelli, F. Martini, A. Milanesi, L. Calucci, M. Geppi, S. Borsacchi, F. Ridi, Effect of phosphate additives on the hydration process of magnesium silicate cements, J. Therm. Anal. Calorim. 138 (2019) 3311–3321, doi:10.1007/s10973-019-08847-9.
[49] Y. Li, D.G. Reid, M.J. Duer, J.C.C. Chan, Solid state NMR - An indispensable tool in organic-inorganic biocomposite characterization; refining the structure of octacalcium phosphate composites with the linear metabolic di-acids succinate and adipate, Solid State Nucl. Magn. Reson. 95 (2018) 1–5, doi:10.1016/j.ssnmr.2018.08.004.
[50] J.V. Bradley, L.N. Bridgland, D.E. Colyer, M.J. Duer, T. Friščić, J.R. Gallagher, D.G. Reid, J.N. Skepper, C.M. Trasler, NMR of biopolymer-apatite composites: developing a model of the molecular structure of the mineral-matrix interface in calcium phosphate biomaterials, Chem. Mater. 22 (2010) 6109–6116, doi:10.1021/cm101730f.
[51] J. Aron-Wisnewsky, J. Doré, K. Clement, The importance of the gut microbiota after bariatric surgery, Nat. Rev. Gastroenterol. Hepatol. 9 (2012) 590, doi:10.1038/nrgastro.2012.161.
[52] B.M. Fung, A.K. Khitrin, K. Ermolaev, An improved broadband decoupling sequence for liquid crystals and solids, J. Magn. Reson. 142 (2000) 97–101, doi:10.1006/jmre.1999.1896.
[53] M.E.A. Cudby, R.K. Harris, K. Metcalfe, K.J. Packer, P.W.R. Smith, A. Bunn, 13C and 1H n.m.r. studies of solid polyolefines, Polymer 26 (1985) 169–176, doi:10.1016/0032-3861(85)90026-6.
[54] E.W. Hansen, P.E. Kristiansen, B. Pedersen, Crystallinity of polyethylene derived from solid-state proton NMR free induction decay, J. Phys. Chem. B. 102 (1998) 5444–5450, doi:10.1021/jp981753z.
[55] A.C. Tas, X-ray-amorphous calcium phosphate (ACP) synthesis in a simple biomineralization medium, J. Mater. Chem. B. 1 (2013) 4511, doi:10.1039/c3tb20854k.
[56] S.V. Dorozhkin, Amorphous calcium orthophosphates: nature, chemistry and biomedical applications, Int. J. Mater. Chem. 2 (2012) 19–46, doi:10.5923/j.ijmc.20120201.04.
[57] C. Drouet, Apatite formation: why it may not work as planned, and how to conclusively identify apatite compounds, BioMed. Res. Int. 2013 (2013) 490946, doi:10.1155/2013/490946.
[58] C. Combes, C. Rey, Amorphous calcium phosphates: Synthesis, properties and uses in biomaterials, Acta Biomater. 6 (2010) 3362–3378, doi:10.1016/j.actbio.2010.02.017.
[59] D.A. Petrash, S.V. Lalonde, M.K. Gingras, K.O. Konhauser, A surrogate approach to studying the chemical reactivity of burrow mucous linings in marine sediments, Palaios 26 (2011) 594–600, doi:10.2110/palo.2010.p10-140r.
[60] C. Holt, M.J.J.M. Van Kemenade, L.S. Nelson, D.W.L. Hukins, R.T. Bailey, J.E. Harries, S.S. Hasnain, P.L. De Bruyn, Amorphous calcium phosphates prepared at pH 6.5 and 6.0, Mater. Res. Bull. 24 (1989) 55–62, doi:10.1016/0025-5408(89)90008-1.
[61] C. Rey, O. Marsan, C. Combes, C. Drouet, D. Grossin, S. Sarda, Characterization of calcium phosphates using vibrational spectroscopies, in: B. Ben-Nissan (Ed.), Adv. Calcium Phosphate Biomater., Springer Berlin Heidelberg, Berlin, Heidelberg, 2014, pp. 229–266, doi:10.1007/978-3-642-53980-0_8.
[62] Y. Kojima, K. Sakama, T. Toyama, T. Yasue, Y. Arai, Dehydration of water molecule in amorphous calcium phosphate, Phosphorus Res. Bull. 4 (1994) 47–52, doi:10.3363/prb1992.4.0_47.
[63] R. Mathew, C. Turdean-Ionescu, Y. Yu, B. Stevensson, I. Izquierdo-Barba, A. García, D. Arcos, M. Vallet-Regí, M. Edén, Proton environments in biomimetic calcium phosphates formed from mesoporous bioactive CaO–SiO $_2$ –P $_2$O 5 Glasses *in Vitro*: insights from solid-state NMR, J. Phys. Chem. C. 121 (2017) 13223–13238, doi:10.1021/acs.jpcc.7b03469.
[64] Y. Wang, S. Von Euw, F.M. Fernandes, S. Cassaignon, M. Selmane, G. Laurent, G. Pehau-Arnaudet, C. Coelho, L. Bonhomme-Coury, M.-M. Giraud-Guille, F. Babonneau, T. Azaïs, N. Nassif, Water-mediated structuring of bone apatite, Nat. Mater. 12 (2013) 1144–1153, doi:10.1038/nmat3787.
[65] S. Von Euw, T.-H.-C. Chan-Chang, C. Paquis, B. Haye, G. Pehau-Arnaudet, F. Babonneau, T. Azaïs, N. Nassif, Organization of bone mineral: the role of mineral-water interactions, Geosciences. 8 (2018) 466, doi:10.3390/geosciences8120466.
[66] W.-Y. Chen, C.-I. Yang, C.-J. Lin, S.-J. Huang, J.C.C. Chan, Characterization of the crystallization pathway of calcium phosphate in liposomes, J. Phys. Chem. C. 118 (2014) 12022–12027, doi:10.1021/jp502428k.
[67] P.S. Belton, R.K. Harris, P.J. Wilkes, Solid-state phosphorus-31 NMR studies of synthetic inorganic calcium phosphates, J. Phys. Chem. Solids. 49 (1988) 21–27, doi:10.1016/0022-3697(88)90129-1.
[68] A. Viani, G. Mali, P. Mácová, Investigation of amorphous and crystalline phosphates in magnesium phosphate ceramics with solid-state 1H and 31P NMR spectroscopy, Ceram. Int. 43 (2017) 6571–6579, doi:10.1016/j.ceramint.2017.02.087.
[69] S. Borsacchi, L. Calucci, M. Geppi, F. La Terra, C. Pinzino, M. Bertoldo, Characterization of an amylose-graft-poly(n-butyl methacrylate) copolymer obtained by click chemistry by EPR and SS-NMR spectroscopies, Carbohydr. Polym. 112 (2014) 245–254, doi:10.1016/j.carbpol.2014.05.086.
[70] V.J. McBrierty, K.J. Packer, Nuclear Magnetic Resonance in Solid Polymers, Cambridge University Press, 1993 http://adsabs.harvard.edu/abs/1993nmrs.book....M (accessed May 27, 2020).
[71] J. Naughton, G. Duggan, B. Bourke, M. Clyne, Interaction of microbes with mucus and mucins, Gut Microbes. 5 (2014) 48–52, doi:10.4161/gmic.26680.
[72] A.P. Corfield, The interaction of the gut microbiota with the mucus barrier in health and disease in human, Microorganisms. 6 (2018), doi:10.3390/microorganisms6030078.
[73] B.O. Schroeder Fight them or feed them: how the intestinal mucus layer manages the gut microbiota Gastroenterol. Rep. 7 2019 3 12 10.1093/gastro/goy052.